24th INTERNATIONAL CONGRESS ON SOUND AND VIBRATION
23–27 July 2017, London

TRANSITION TO TURBULENCE IN OSCILLATING FLOWS

Islam. A. Ramadan[1,4], Ahmed. I. Abd El-Rahman[2], A. H. Ibrahim[1,3]
[1] *School of Science and Engineering, American University in Cairo, P.O. Box 74, New Cairo 11835, Egypt.*
[2] *The Department of Mechanical Power Engineering, Cairo University, Giza 12613, Egypt.*
[3] *On leave from The Department of Mechanical Power Engineering, Cairo University, Giza 12613, Egypt.*
[4] *Email: islamramadan@aucegypt.edu*

Ehab Abdel-Rahman
Professor of Physics, Department of Physics, The American University in Cairo, 11835 New Cairo, Egypt

Non-linearities associated with the oscillating flow contribute in deteriorating the performance of thermoacoustic systems. Turbulence generation is one of these non-linearities which dissipates the acoustic energy into a non-useful form of energy (heat). In this work, the transition to turbulence in oscillating flow inside a square duct is investigated experimentally. The axial velocity profile is measured using Particle Image Velocimetry and the oscillatory Reynolds number is used to characterize the oscillating flow. At low Reynolds number, the measured cross sectional axial velocity profile in the duct agrees reasonably well with the theoretical laminar velocity profile over the complete cycle; whereas at higher Reynolds number, the results show that the agreement becomes limited to the acceleration phase. As the Reynolds number increases, the portion of the cycle over which the agreement between the measurements and theory occurs decreases. The measured turbulence intensity and the Reynolds shear stress are used to characterize the transition to turbulence process. The turbulence intensities based on both velocity components over the half width of the duct increase as the Reynolds number is increased. Also, the turbulence intensities have maximum values near to the wall. Beyond a certain Reynolds number, the Reynolds shear stress experiences a sudden increase indicating transition to turbulence and hence the value of the critical Reynolds number can be determined. The estimated value of the critical Reynolds number agrees well with the literature.
Keywords: oscillating flow, transition to turbulence, particle image velocimetry, thermoacoustics.

1. Introduction

In general, the oscillating flow can be divided into two major types: namely, pulsatile flow and pure oscillating flow. The pulsatile flow is an oscillating flow superimposed on a steady flow with a non-zero mean velocity, whereas the pure oscillating flow is an oscillating flow with zero mean velocity. The latter type of the oscillating flows is the main concern of this study. The understanding of the physics underlying the transition to turbulence in oscillating flow is an important issue for many engineering applications.

The laminar oscillating flow in circular ducts has been studied experimentally and well understood. In addition, many theoretical studies have been developed to describe the laminar oscillating flow in circular ducts at different conditions and they agree well with the experimental data [1] and [2]. The oscillating flow in rectangular ducts has been studied theoretically [3], [4] and [5]. However, the experimental studies validating these theoretical studies are scarce.

The transition to turbulence characterizes the end of the laminar regime. Generally, the values of both the Reynolds number (Re_D) and Womersley number (α) are used to specify the extent of the laminar regime, which are defined as:

$$Re_D = \frac{U_o D_h}{\upsilon} \; and \; \alpha = \frac{D_h/2}{\sqrt{\upsilon/(2\pi f)}},$$

where U_o is the centreline axial velocity amplitude, D_h is the hydraulic diameter of the duct, υ is the kinematic viscosity and f is the frequency of the oscillating flow. These two non-dimensional parameters can be combined in one non-dimensional parameter which is the oscillatory Reynolds number as is defined as follows:

$$Re_\delta = \frac{U_o \delta}{\upsilon},$$

where ($\delta = \sqrt{\frac{2\upsilon}{2\pi f}}$) is the viscous penetration depth.

The previous investigations showed different values for the critical Reynolds number. Although the Reynolds number Re_δ includes the effect of the frequency, it was found that the value of the critical Reynolds number depends on the frequency range. At high frequency range (i.e. acoustic frequencies, higher than 20 Hz), Merkli *et al.* [6] found that the value of the critical Reynolds number is 280, whereas at sub-acoustic frequencies the value was found to be 500 [7], [8].

Many experimental and theoretical studies attempted to characterize the transition to turbulence regime. Collins [9] used instability theory to determine the first instability point in the boundary layer of the oscillating flow and he concluded that the instability is originated during the acceleration phase. However, his theoretical expectation was not in agreement with the experimental measurements where [10] and [11] observed that the turbulence bursts appear during the deceleration phase.

In all of the previous measurements intrusive techniques such as hot-wire were utilized and hence the evaluation for those techniques was necessity. Eckmann *et al.* [12] studied the effects of the intrusion of hot-wire probe in the oscillating flow using LDV. They found that the existence of the hot-wire probe leads to instabilities in the boundary layer at Reynolds number of 300 whereas the instabilities started at Reynolds number of 500 when the probe is removed. Also, Merkli *et al.* [6] concluded that the hot-wire measurements in the boundary layer at high frequencies are misleading because the size of boundary layer at high frequencies becomes too small and hence the disturbance of the hot-wire probe becomes large enough to affect the collected data.

Since Laser Doppler Velocimetry (LDV) technique became more reliable on such measurements, it has been utilized in many studies in which the authors attempted to shed light on the generation of turbulence during the cycle. Flisher *et al.* [13] described different flow structures and events that are responsible for the turbulence generation in the oscillating flow. These events are not random in time and space in contrast to steady flow turbulence and they occurred mainly during the deceleration phase. In addition, they defined a range for the value of critical Reynolds number ($650 < Re_\delta < 1000$). Akhavan *et al.* [14] concluded that the turbulent boundary layer of the oscillating flow consists of the same layers of the turbulent steady flow which are a viscous sublayer, a logarithmic layer and an outer wake. Reyt *et al.* [2] observed that the value of the viscous boundary layer thickness becomes larger than the theoretical value as the Reynolds number is increased.

Although the Particle Image Velocimetry (PIV) has the advantage of getting the spatial velocity distribution instantaneously and hence gives better understanding for the flow structures when compared with other techniques, the limited sampling frequency (up to 10 Hz) of its old versions resulted in limited PIV studies in this field. Currently, the sampling frequencies of the PIV systems reached up to 10 kHz. In this work, time-resolved PIV system is utilized to study the transition to turbulence in oscillating flow inside square duct. In section 2, the experimental setup is explained and the data analysis method is described as well. In section 3, the results are presented and discussed. In section 4, the work is summarized and conclusions are drawn.

2. Procedure

2.1 Experimental setup

The experimental setup was designed to achieve wide range of both the Reynolds number $(140 < Re_\delta < 600)$ and the Womersley number $(10 < \alpha < 17)$. As shown in Fig. 1, the oscillating flow is driven by a pneumatic piston-cylinder assembly (JELPC, Model: S125X300) with piston diameter of 125 mm and with a stroke limit of 300 mm. The piston is connected to Scotch-Yoke mechanism that converts the rotary motion of a 4-kw electric motor (ELMA-TROYAN, Model: T 132MA 6 B3) to a reciprocating motion. The motor frequency is controlled by a variable-speed drive (Schneider-Electric, Model: ATV312HU40N4). The stroke limit can be varied from 70 mm to 200 mm by changing the pin location on the flywheel.

In all experiments, the duct is filled with air at the atmospheric pressure and temperature. The oscillating flow is delivered to the resonator from both sides through flexible pipes. The resonator is made of stainless-steel square duct with inner side length (W) of 45 mm, thickness of 3 mm and length of 1900 mm. The measurement section is a square glass tube that has the same inner side length of the resonator and a length of 500 mm and placed in the middle of the resonator. To eliminate the end-effects, two flow straighteners are placed at both ends of the resonator each is made of 100 CPSI (cell per square inch) ceramic stack and with a length of 25 mm. Because, Gerrard *et al.* [15] proved that the oscillating flow is considered to be fully developed at length $(L) = 0.03 * D_h * Re_\delta$ and hence the longest expected entrance length, based on maximum laminar Reynolds number of 500, is estimated as 660 mm. So, the measurement section is placed at distance of 700 mm from both ends of the resonator. It should be noted that the origin of the axes (x, y and z) is located at the middle-centre of the duct.

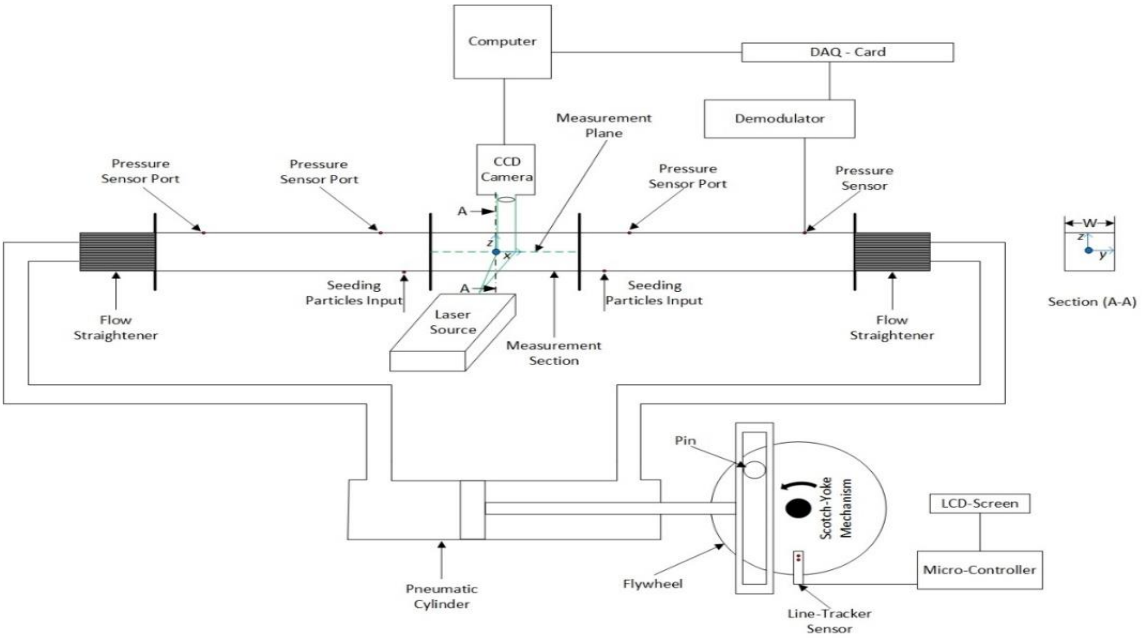

Figure 1: Schematic for the experimental setup including the measurement systems and the mechanism used to generate the oscillating flow.

2.2 PIV measurements and data processing

Time-resolved PIV system is used in this study. The system is supplied by Dantec-Dynamics and consists of Nd:YLF green laser (wavelength of 527 nm). The CCD-camera (Photron SA1.1, maximum frame rate of 5400 frames/s at full resolution of 1024 X 1024 Pixels^2, connected to 60 mm Nikon AF macro prime lens) is utilized to capture and record the images of the seeded flow. The seeding particles, delivered to the measurement section, are produced by a jet-atomizer (TSI Model

9306) that produces particles with a mean diameter of 0.6 μm. Finally, the timer box (National Instruments Model 80N77) is used to synchronize the laser light pulses and the CCD camera and it is externally triggered by a TTL signal provided by the line tracker (IR sensor) in order to start measurements at a defined phase in the cycle. Total number of $A = 50$ flow fields are captured per one cycle and the measurements last for $B = 50$ successive cycles and hence the total number of images is 2500. The time between pulses is adjusted to allow the seeding particles to move a distance nearly equal to a quarter of the interrogation window length.

The method of analysing the measured data to get the velocity distribution over the cross section is quite similar to the method used in [16]. The velocity vectors in each map is spatially averaged along the x-direction because the velocity is almost constant in that direction. Then, phase averaging is implemented to get the velocity distribution over one cycle.

A graphical representation for the method of the analysis is depicted in Fig. 2. The total number of vectors in each map is $N\ times\ M$, where $N\ and\ M$ are the total number of interrogation areas in x direction and y direction and equals to 127 and 127, respectively. The total number of maps indexed from $i = 1$ to $i = AXB$. The velocity vector at each interrogation area within the velocity map can be expressed as following

$$\boldsymbol{U_i(n,m)}, \tag{1}$$

where the velocity vector $U_i(n,m)$ includes both x-direction $u_i(n,m)$ and y-direction $v_i(n,m)$ velocity components. Then, the velocity vectors at the same y-position are averaged along x-axis and hence the spatial-average velocity distribution can be expressed as

$$\bar{\mathbf{U}}_{\boldsymbol{i}}(\boldsymbol{m}) = \frac{\mathbf{1}}{\boldsymbol{N}}\sum_{\boldsymbol{n=1}}^{\boldsymbol{N}} \boldsymbol{U_i(n,m)} \tag{2}$$

Finally, the maps of those 50 cycles are averaged to get the phase-average velocity vector distribution over one cycle that can be expressed as

$$\bar{\bar{\boldsymbol{U}}}_{\emptyset}(\boldsymbol{m}) = \frac{\mathbf{1}}{\boldsymbol{B}}\sum_{\boldsymbol{i=0}}^{\boldsymbol{B-1}} \boldsymbol{U_{Ai+\emptyset}(m)} \tag{3}$$

where $\emptyset$ is the phase number in the cycle and is ranged from $\emptyset = 1$ to $\emptyset = A$.

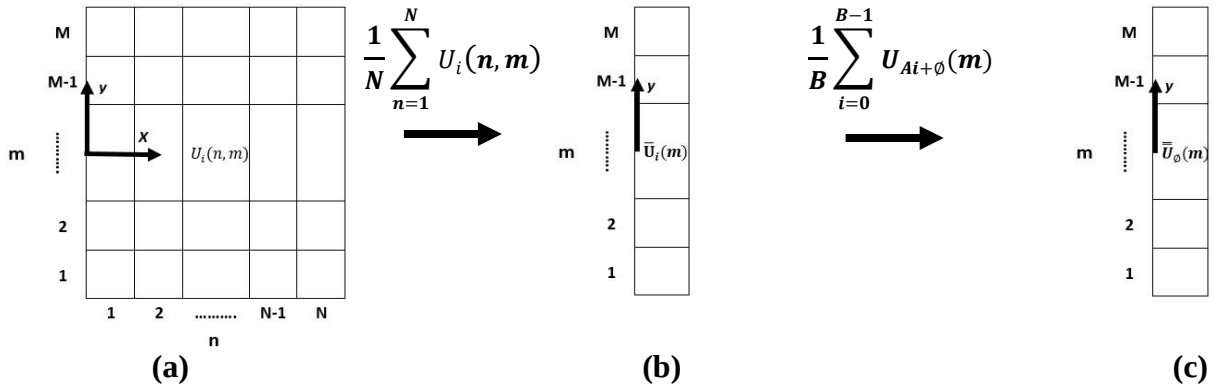

Figure 2: (a) An example for velocity vectors map. (b) Spatial-average velocity distribution. (c) Phase-average velocity distribution.

3. Results and discussion

In this study, nine experiments at different operating conditions are conducted. The operating conditions for each experiment are presented in Table 1. As mentioned in the previous section, the total number of phases per cycles is fifty and the number of the averaged-cycles per phase is fifty as well. In order to make sure that the used number of averaged images per phase is enough for the stationarity of the measured mean velocity; the number of averaged-cycles is changed and its effects are investigated. As shown in Fig. 3, as the number of averaged-cycles is increased, the value of the mean velocity at any phase becomes nearly constant. It is found that the number of cycles required to get a

stable mean velocity data is more than 30 cycles at a high Reynolds number. However, the 30-cycles criterion may be insufficient for the stability of the higher moment like velocity fluctuations and hence the turbulence intensities based on x and y velocity components are calculated using different numbers of averaged-cycles (B). The turbulence intensities based on x and y velocity components at any phase, $\boldsymbol{I_{x_\emptyset}}$ and $\boldsymbol{I_{y_\emptyset}}$, respectively can be calculated as follows:

$$\boldsymbol{I_{x_\emptyset}(m) = \sqrt{\frac{1}{B}\sum_{i=0}^{B-1}[\overline{u}_{Ai+\emptyset}(m) - \overline{\overline{u}}_\emptyset(m)]^2}} \quad \textbf{(4)}$$

$$\boldsymbol{I_{y_\emptyset}(m) = \sqrt{\frac{1}{B}\sum_{i=0}^{B-1}[\overline{v}_{Ai+\emptyset}(m) - \overline{\overline{v}}_\emptyset(m)]^2}} \quad \textbf{(5)}$$

Table 1: The operating conditions for each experiment

Experiment #	f (Hz)	U_o (m/s)	δ (mm)	Re_δ	α
1	0.5	0.7	3.16	141	10
2	1	1.4	2.2	196	14.2
3	1.5	2.0	1.8	230	17.4
4	0.5	1.3	3.16	262	10
5	1	2.5	2.2	350	14.2
6	1.5	3.6	1.8	412	17.4
7	0.5	2.2	3.16	442	10
8	1	3.5	2.2	490	14.2
9	1.25	4.0	2.0	510	16

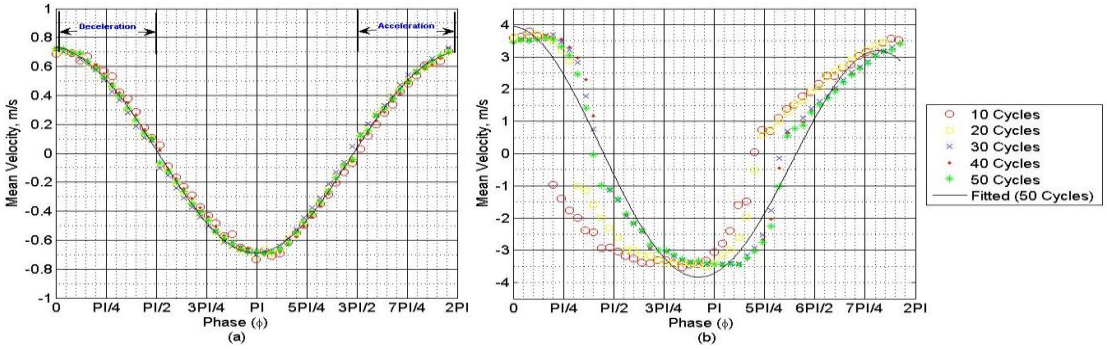

Figure 3: The effect of the number of the averaged-images on the value of the mean velocity over the cycle at two different Reynolds numbers: (a) Experiment# 1 and (b) Experiment# 8

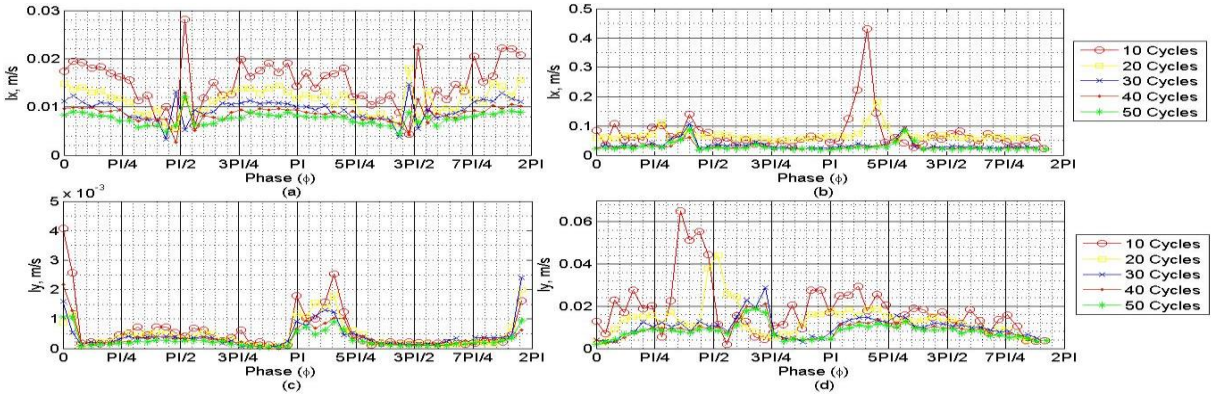

Figure 4: The effect of the number of the averaged-images on the values of the turbulence intensities (based on x and y velocity components) over the cycle at the centre of the duct ($y = 0$) at two different experimental conditions: (a, c) Experiment# 1 and (b, d) Experiment# 8.

As shown in Fig. 4, the values of the turbulence intensities over the cycle becomes stable when the number of the averaged-cycles exceeds 40 images; and hence 50 images are sufficient to get converged velocity data which is in agreement with the findings of [16]. Hereinafter, the presented data are based on averaging 50 cycles.

3.1 Laminar flow regime and validation

In order to validate the measurement procedure explained above; the measured distribution of the axial velocity over the half width of the duct is compared with the theoretical expectations derived in [5]. As the theoretical expectations were derived for the flow in the laminar regime; the comparison is done at the lowest Reynolds number (Exp.#1). As shown Fig. 5 (Exp.#1), there is a good agreement between the measured and the theoretical values over the whole cycle. It should be noted that the positive half of the cycle is only considered since the negative and positive halves are identical.

3.2 Transition to turbulence regime

In order to recognize the end of the laminar regime; the measured distributions of the axial velocity at different Reynolds numbers are compared with the theoretical expectations. As shown in Fig. 5, as the Reynolds number is increased up to 230; the measured values agree well with the theoretical expectations over the whole cycle. For Reynolds number higher than 230, the agreement with theory is valid over the whole cycle except at the deceleration phase ($\emptyset = \pi/4$). This behaviour is observed up to Reynolds number of 412. For Reynolds number higher than 412, it is observed that the deviation from theory in the boundary layer extends to the acceleration phases as well. For Reynolds number higher than 500, there is a large deviation from theory in the boundary layer at the phases where the velocity direction is reversed. Also, the discontinuity in the velocity distribution at these phases may be due to the increase of the acceleration error associated with PIV technique.

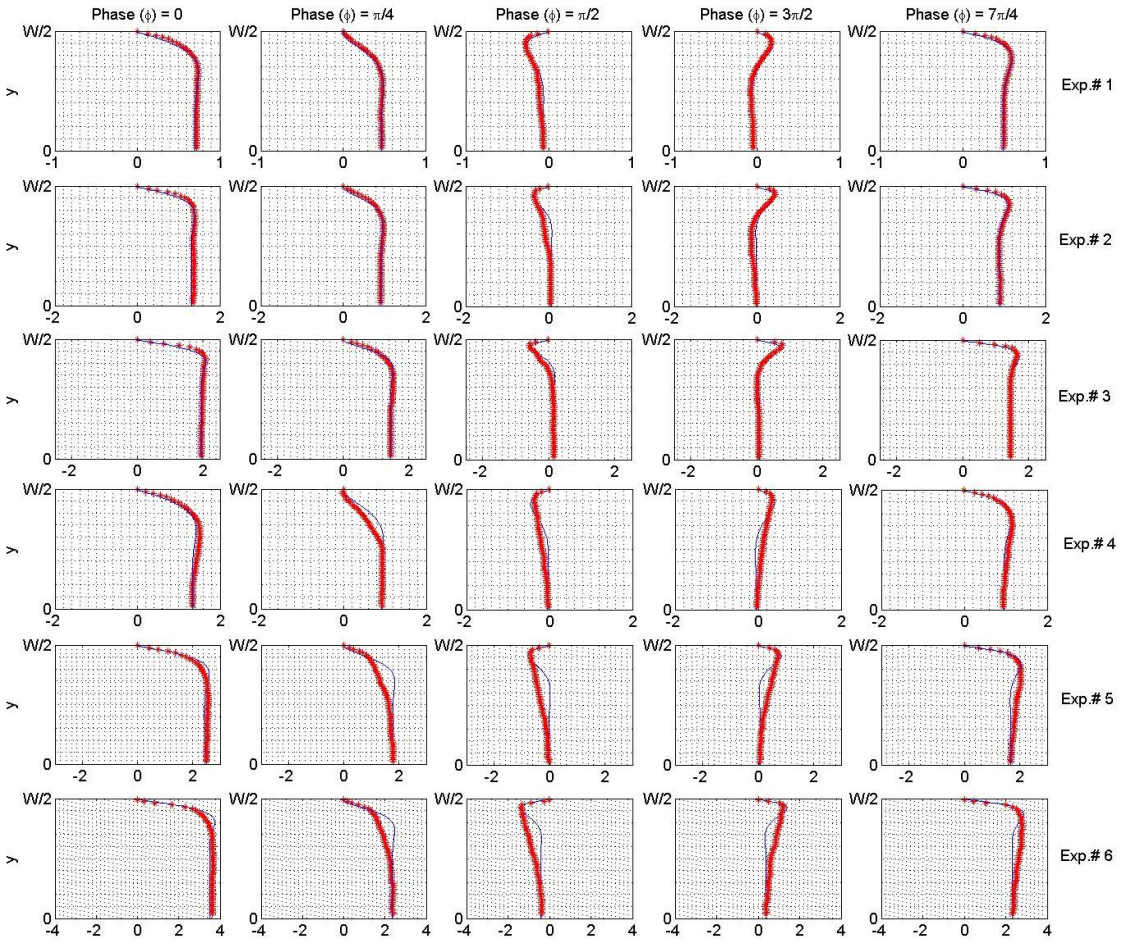

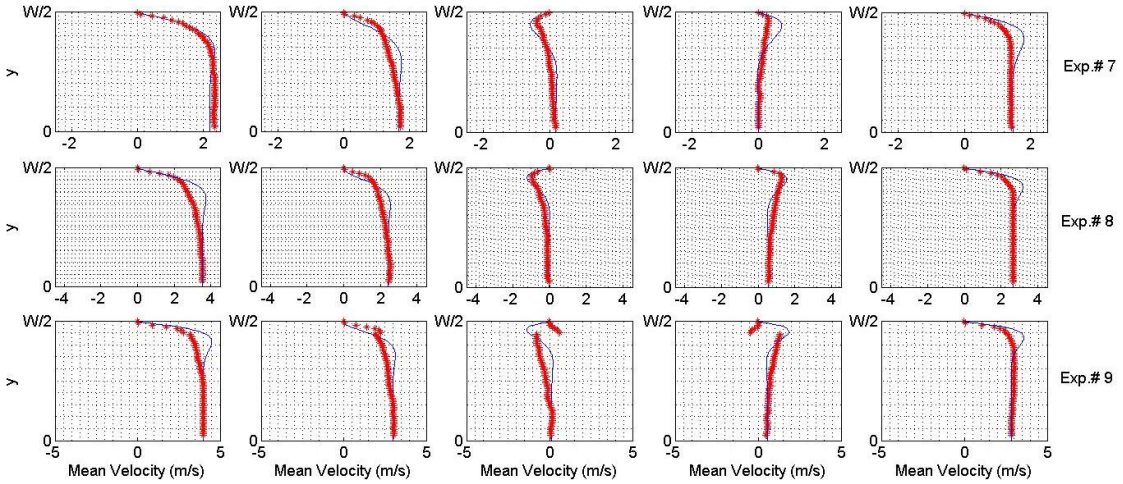

Figure 5: The measured (*) and the theoretical (—) distributions of the axial velocity over the half width of the duct at different phases during the cycle at different experimental conditions.

The phase-average turbulence intensities in both directions normalized by the centreline axial velocity amplitude (U_o) are calculated. Also, the value of the Reynolds shear stress divided by the flow density is calculated as follows:

$$Re_{stress_{\emptyset}}(m)/\boldsymbol{\rho} = \frac{1}{B}\sum_{i=0}^{B-1}[\bar{u}_{Ai+\emptyset}(m) - \bar{\bar{u}}_{\emptyset}(m)] * [\bar{v}_{Ai+\emptyset}(m) - \bar{\bar{v}}_{\emptyset}(m)] \quad \textbf{(6)}$$

As shown in Fig. 6a, the phase-average turbulence intensity based on x-velocity component increases as the Reynolds number is increased. Also, the maximum value is achieved near to the wall rather than the centre of the duct. In Fig. 6b, the phase-average turbulence intensity based on y-velocity component increases as the Reynolds number is increased. In Fig. 6c, the phase-average Reynolds stress divided by the density increases as the Reynolds number is increased. Also, it is obvious that the value of the phase-average Reynolds stress increases significantly when the Reynolds number exceeds 500. The sharp increase in the value of the Reynolds stress beyond a certain value of Reynolds number indicates the transition to turbulence process. So, it can be concluded that the critical Reynolds number is about 500 which is in agreement with the literature [7], [8].

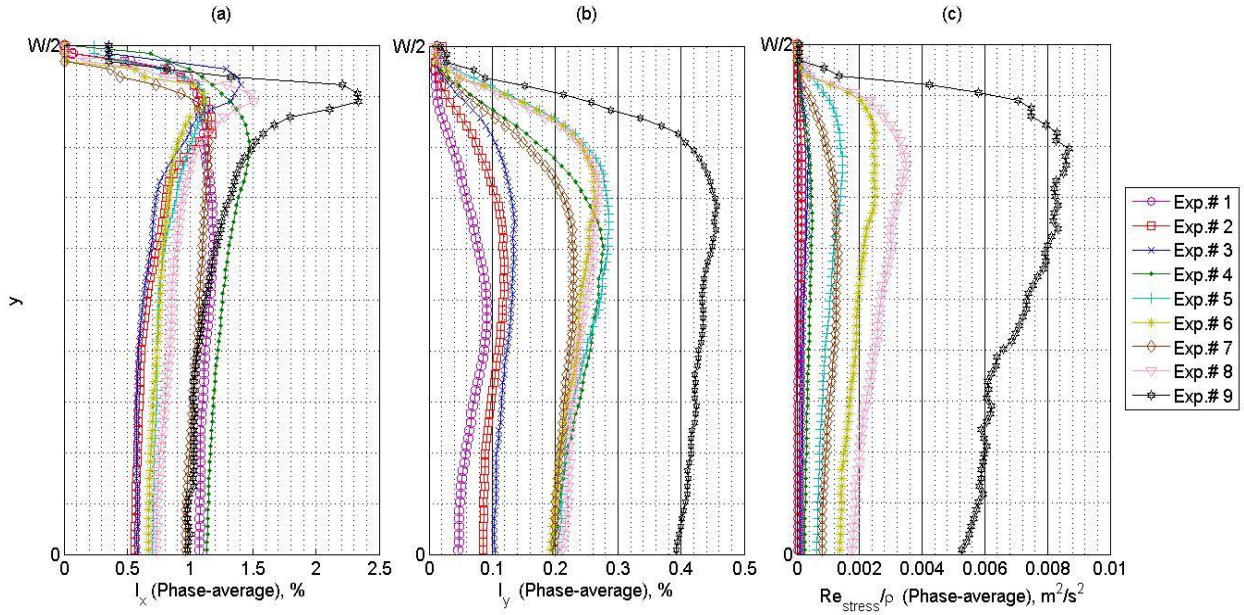

Figure 6: The distribution of the Phase-average turbulence intensity normalized by the centreline axial velocity amplitude over the half width of the duct based on: (a) x-velocity component and (b) y-velocity component. (c) The distribution of the phase-average Reynolds stress divided by the density over the half width of the duct.

4. Conclusions

The transition to turbulence in oscillating flow has been investigated experimentally using time resolved PIV measurements. The axial velocity distribution in a square duct is measured at different Reynolds number and Womersley number and compared with the theoretical expectations. At low Reynolds number, the measured values are in agreement with the theoretical expectations. As the Reynolds number is increased; the agreement is violated in the deceleration phase first and then in more phases in the cycle. At the critical Reynolds number around 500, it is observed that there is a lump in the level of the axial turbulence intensity.

Acknowledgement

This publication has been produced with the financial assistance of the European Union. The contents of this document are the sole responsibility of the authors and can under no circumstances be regarded as reflecting the position of the European Union.

REFERENCES

[1] M. Hino, M. Sawamoto and S. Takasu, "*Experiments on transition to turbulence in an oscillatory pipe flow*," *Journal of fluid mechanics,* vol. **75**, no. 2, pp. 193-207, 1976.

[2] I. Reyt, H. Bailliet, E. Foucault and J.-C. Valiere, "*Oscillating Viscous Boundary Layer at High Reynolds Number: Experiments and Numerical Calculations,*" in *20th ISNA*, Lyon, France, 2015.

[3] D. G. Drake , "*On the flow in the channel due to a periodic pressure gradient*," *Quart. Jonrn. Mech and Applied Math.,* vol. **XVIII**, 1963.

[4] S. Tsangaris, "*Exact Solution of the Navier-Stokes Equations for the Fully Developed, Pulsating Flow in a Rectangular Duct With a Constant Cross-Sectional Velocity*," *Journal of fluids engineering* , vol. **125**, pp. 382-392, 2003.

[5] C. FAN, "*Unsteady, Laminar, Incompressible Flow Through Rectangular Ducts*," *Journal of Applied Mathematics and Physics,* vol. **16**, pp. 351-360, 1965.

[6] P. Merkli and H. Thomann, "*Transition to turbulence in oscillating pipe flow*," *Journal of fluid mechanics,* vol. **68**, no. 3, pp. 567-575, 1975.

[7] S. I. Sergeev, "*Fluid oscillations in pipes at moderate Reynolds numbers*," *Fluid Mechanics* , vol. **1**, no. 1, pp. 121-122, 1966.

[8] M. Ohmi and M. Iguchi, "*Critical Reynolds number in an oscillating pipe flow*," *Bulletin of JSME,* vol. **25**, no. 200, 1982.

[9] J. I. Collins, "*Inception of turbulence at the bed under periodic gravity waves*," *Journal of Geophysical Research,* vol. **68**, no. 21, pp. 6007-6014, 1963.

[10] T. S. Zhao and P. Cheng, "*Experimental studies on the onset of turbulenceand frictional losses in an oscillatory turbulent pipe flow*," *International journal of heat and fluid flow,* vol. **17**, pp. 356-362, 1996.

[11] M. Hino, M. Kashiwayanagi, A. Nakayama and T. Hara, "*Experiments on the turbulence statistics and the structure of a reciprocating oscillatory flow*," *Journal of fluid mechanics,* vol. **131**, pp. 363-400, 1983.

[12] M. Eckmann and J. B. Grotberg, "*Experiments on transition to turbulence in oscillatory pipe flow*," *Journal of Fluid Mechanics,* vol. **222**, pp. 329-350, 1991.

[13] L. S. Fishler and R. S. Brodkey, "*Tansition, turbulence and oscillating flow in a pipe*," *Experiments in fluids,* vol. **11**, pp. 388-398, 1991.

[14] R. Akhavan, R. D. Kann and A. H. Shapiro, "*An investigation to turbulence in bounded oscillatory stokes flows Part 1. experiments*," *Journal of fluid mechanics* , vol. **225**, pp. 398-422, 1991.

[15] J. H. Gerrard and M. D. Hughes, "*The flow due to an oscillating piston in a cylindrical tube: a comparison between experiment and a simple flow theory*," *Journal of fluid mechanics,* vol. **50**, no. 1, pp. 97-106, 1971.

[16] R. Trip, D. J. Kuik, J. Westerweel and C. Poelma, "*An experimental study of transitional pulsatile pipe flow*," *Physics of Fluids,* vol. **24**, 2012.